# SIMULTANEOUS *SWIFT* AND REM MONITORING OF THE BLAZAR PKS 0537−441 IN 2005

E. Pian,[1] P. Romano,[2,3] A. Treves,[4] G. Ghisellini,[2] S. Covino,[2] A. Cucchiara,[5] A. Dolcini,[4]
G. Tagliaferri,[2] C. Markwardt,[6] S. Campana,[2] G. Chincarini,[2,3] N. Gehrels,[6]
P. Giommi,[7] L. Maraschi,[8] S. D. Vergani,[9,10] F. M. Zerbi,[2] E. Molinari,[2] V. Testa,[11]
G. Tosti,[12] F. Vitali,[11] L. A. Antonelli,[11] P. Conconi,[2] G. Malaspina,[2]
L. Nicastro,[13] E. Palazzi,[13] E. J. A. Meurs,[9] and L. Norci[10]

## ABSTRACT

The blazar PKS 0537−441 has been observed with all instruments of the *Swift* satellite between the end of 2004 and 2005 November. The BAT monitored it recurrently for a total of 2.7 Ms, and the XRT and UVOT pointed it on seven occasions for a total of 67 k. The automatic optical and near-infrared telescope REM has monitored simultaneously the source at all times. In 2005 January–February, PKS 0537−441 was detected at its brightest in optical and X-rays: more than a factor of 2 brighter in X-rays and about a factor of 60 brighter in the optical than observed in 2004 December. The 2005 July observation recorded a fainter X-ray state, albeit still brighter than the historical average. The simultaneous optical state is comparable to the one recorded in early 2005 January, before the outburst. In 2005 November, the source subsided both in X-rays and optical to a quiescent state. The optical and X-ray variations are well correlated, with no measurable time lag larger than about 1 month. On intraday timescales there is no obvious correlation between X-ray and optical variations, but the former tend to be more pronounced, opposite to what is observed on monthly timescales. The widely different amplitude of the long-term variability in optical and X-rays is very unusual. The spectral energy distributions are interpreted in terms of the synchrotron and inverse Compton mechanisms within a jet where the plasma radiates via internal shocks and the dissipation depends on the distance of the emitting region from the central engine.

*Subject headings:* BL Lacertae objects: individual (PKS 0537−441) — galaxies: active — gamma rays: observations — radiation mechanisms: nonthermal

*Online material:* color figure

## 1. INTRODUCTION

Multiwavelength variability is the most effective diagnostic tool of the properties of extragalactic jets and of their central engines. Due to the orientation of their jets—nearly aligned to our line of sight—blazars allow a better insight into their inner regions than other radio-loud active galactic nuclei (AGNs) do, because the intrinsic flux variability is magnified by relativistic effects. Past observations of blazars have identified the active emission mechanisms (synchrotron process at frequencies up to the soft, and occasionally hard, X-rays and inverse Compton scattering at higher energies; Ulrich et al. 1997; Pian et al. 1998; Tagliaferri et al. 2003; Krawczynski et al. 2004; Dermer & Atoyan 2004; Błażejowski et al. 2005; Sokolov & Marscher 2005; Aharonian et al. 2006; Albert et al. 2006; Kato et al. 2006; Massaro et al. 2006; Raiteri et al. 2006). Yet, the structure of the jet, the mechanisms of the energy transfer from the central engine to the emitting particles, and the dissipation processes along the jet are not clear. Intensive monitorings and good coverage at all frequencies are necessary to explore the multiwavelength variability of blazars to its full extent and to understand how the jet interacts with other circumnuclear components to produce the radiation. The *Swift* satellite (Gehrels et al. 2004), with its easy and flexible scheduling, can be optimally employed for the observation of bright blazars (Giommi et al. 2006; Sambruna et al. 2006; Tramacere et al. 2007).

The blazar PKS 0537−441 ($z = 0.896$) is a bright emitter at all frequencies from radio to gamma rays. In the latter band it has been observed many times by EGRET and detected in different states (Treves et al. 1993; Hartman et al. 1999; Pian et al. 2002). The source was targeted for long-term optical and near-IR monitoring with the automatic optical/near-IR 60 cm telescope Rapid Eye Mount (REM; Zerbi et al. 2001; Chincarini et al. 2003; Covino et al. 2004) in 2004 December–2005 March, when the blazar exhibited a flare with a timescale of about a month (Dolcini et al. 2005). At that time, *Swift* had observed PKS 0537−441 for calibration purposes. On 2005 June 25, the *RXTE* All Sky Monitor recorded a high X-ray (2–10 keV) state of the source, with a flux of $(13 \pm 5)$ millicrab. The REM monitoring in the optical also revealed the blazar to be active (Covino et al. 2005). Based on these alerts, we requested observations of PKS 0537−441 as a target of opportunity with *Swift*. A first observation was scheduled in 2005 July. A second *Swift* visit took place in 2005 November, in order to monitor the long-term behavior of the source after the 2005 June outburst. We report here the results of all *Swift*

[1] INAF−Trieste Astronomical Observatory, 34143 Trieste, Italy.
[2] INAF−Brera Astronomical Observatory, 23807 Merate (LC), Italy.
[3] Department of Physics, University of Milano-Bicocca, 20126 Milan, Italy.
[4] Department of Physics and Mathematics, University of Insubria, 22100 Como, Italy.
[5] Department of Astronomy and Astrophysics, Pennsylvania State University, University Park, PA 16802.
[6] NASA Goddard Space Flight Center, Greenbelt, MD 20771.
[7] ASI Science Data Center, ASDC c/o ESRIN, 00044 Frascati, Italy.
[8] INAF−Brera Astronomical Observatory, 20121 Milano, Italy.
[9] Dunsink Observatory–DIAS, Dublin 15, Ireland.
[10] School of Physical Sciences and NCPST, Dublin City University, Dublin 9, Ireland.
[11] INAF−Rome Astronomical Observatory, 00040 Monte Porzio Catone, Italy.
[12] Department of Physics, University of Perugia, Perugia, Italy.
[13] INAF−Institute of Space Astronomy and Cosmic Physics, 40129 Bologna, Italy.

TABLE 1
*Swift* XRT Observation Log

| Start Time (UT) | End Time (UT) | Exposure (s) | Mean Flux[a] (0.5–10 keV) | Counts (0.2–10 keV) | Spectral Index | $\chi^2_{\rm red}$ (dof) C-stat (%) |
|---|---|---|---|---|---|---|
| 2004 Dec 23 23:37:34........... | 2004 Dec 23 23:59:40 | 1029 | $0.67^{+0.83}_{-0.50}$ | 168 | $0.75 \pm 0.18$ | 372.7 (32.2)[b] |
| 2005 Jan 27 00:05:19............ | 2005 Jan 27 22:37:41 | 7248 | $1.49^{+0.10}_{-0.08}$ | 2660 | $0.73 \pm 0.05$ | 1.06 (101) |
| 2005 Jan 28 00:08:16............ | 2005 Jan 28 23:03:41 | 22663 | $1.38 \pm 0.05$ | 7794 | $0.76 \pm 0.03$ | 1.12 (244) |
| 2005 Feb 24 16:19:51 .......... | 2005 Feb 25 12:00:40 | 18592 | $1.26 \pm 0.05$ | 5420 | $0.65 \pm 0.03$ | 0.99 (198) |
| 2005 Jul 12 01:13:01............. | 2005 Jul 12 11:12:59 | 4977 | $1.05 \pm 0.11$ | 1003 | $0.57 \pm 0.07$ | 0.93 (44) |
| 2005 Nov17 00:45:12............ | 2005 Nov 17 12:11:11 | 6373 | $0.39 \pm 0.06$ | 556 | $0.75^{+0.11}_{-0.10}$ | 1.16 (23) |
| 2005 Nov 24 22:14:00 .......... | 2005 Nov 25 11:25:57 | 6243 | $0.44^{+0.07}_{-0.06}$ | 583 | $0.77 \pm 0.10$ | 1.00 (24) |

Note.—All observations were carried out with XRT in PC observing mode.
[a] Unabsorbed flux in units of $10^{-11}$ ergs cm$^{-2}$ s$^{-1}$. The effects of PSF-loss and vignetting were taken into account in the count rate to flux conversion.
[b] Cash statistic (C-stat) and percentage of Monte Carlo realizations that had statistic <C-stat, for this entry only.

observations of PKS 0537−441, and of the simultaneous REM observations in 2005 July and 2005 November.

## 2. DATA ACQUISITION, REDUCTION, AND ANALYSIS

### 2.1. *X-Ray Observations*

#### 2.1.1. *Swift BAT*

PKS 0537−441 was often in the field of view of the *Swift* Burst Alert Telescope (BAT; 15–150 keV) from 2004 December to 2005 November. The BAT data were analyzed using the standard BAT analysis software distributed within FTOOLS version 6.0.5. Although the blazar is not detected in individual *Swift* orbits by BAT, averaging the BAT signal during all periods of observation results in significant flux detection. A spectrum of the integrated data set was extracted and fitted to a single power law $F_\nu \propto \nu^{-\beta}$ with spectral index $\beta = 0.5 \pm 0.5$ (reduced $\chi^2 = 1.03$). The flux in the 15–150 keV band is $(3.2^{+0.9}_{-2.3}) \times 10^{-11}$ ergs cm$^{-2}$ s$^{-1}$.

#### 2.1.2. *Swift XRT*

The blazar was observed with the X-Ray Telescope (XRT; 0.2–10 keV; Burrows et al. 2005) in 2004 December–2005 February, 2005 July, and 2005 November. The monitoring is organized in seven observations, four of which were obtained during the *Swift* XRT calibration phase. The XRT data were first processed by the *Swift* Data Center at NASA/GSFC into level 1 products (calibrated and quality-flagged event lists). Then they were further processed with the latest Heasoft release[14] (ver. 6.0.5) to produce the final cleaned event lists. In particular, we ran the task `xrtpipeline` (ver. 0.10.3) applying standard filtering and screening criteria, i.e., we cut out temporal intervals during which the CCD temperature was higher than $-47^\circ$C, and we removed hot and flickering pixels, which are present because the CCD is operating at a temperature higher than the design temperature of $-100^\circ$C due to a failure in the active cooling system. An on-board event threshold of ∼0.2 keV was also applied to the central pixel, which has been proven to reduce most of the background due to either the bright Earth limb or the CCD dark current (which depends on the CCD temperature). Given the low rate of PKS 0537−441 during the observing campaign (<0.5 counts s$^{-1}$ in the 0.2–10 keV range), we only considered photon counting (PC) data for our analysis (see Hill et al. 2004 for a full description of read-out modes) and further selected XRT grades 0–12, (according to *Swift* nomenclature; Burrows et al. 2005). A summary of the XRT observations is reported in Table 1.

[14] See http://swift.gsfc.nasa.gov/docs/software/lheasoft.

PKS 0537−441 was detected in the XRT data at the coordinates R.A. = 05h38m50.38s, decl. = $-44^\circ05'09.1''$ (J2000.0), with an estimated uncertainty of 3.5″ radius (90% containment). This position takes into account the correction for the misalignment between the telescope and the satellite optical axis (Moretti et al. 2006), and is consistent with the source catalog position (ICRS coordinates are R.A. = 05h38m50.36s, decl. = $-44^\circ05'08.94''$).

We extracted the source events in a circle with a radius of 30 pixels (∼71″), which corresponds to ∼94% of the XRT PSF. To account for the background, the data were also extracted within an annular region (radii 55 and 95 pixels) centered on the source and devoid of background sources.

The source and background spectra were extracted in the regions described above. Ancillary response files were generated with the task `xrtmkarf`, and account for differences in extraction regions and PSF corrections. We used the latest spectral redistribution matrices (RMF, v008). The adopted energy range for spectral fitting is 0.3–10 keV, and all data were rebinned with a minimum of 20 counts per energy bin to allow $\chi^2$ fitting within XSPEC (ver. 11.3.2). The only exception was the observation of 2004 December 23, when the number of counts was limited (∼140) and Cash (1979) statistics was appropriate; therefore ungrouped data were used instead.

The spectra do not exhibit significant features, either in absorption or in emission, superimposed on the power-law continuum (see a representative spectrum in Fig. 1). We considered an absorbed power-law model, with the neutral hydrogen column kept fixed to its Galactic value ($2.91 \times 10^{20}$ cm$^{-2}$; Murphy et al. 1996), and the spectral index left as a free parameter. The fit results are reported in Table 1.

### 2.2. *Optical Observations*

The *Swift* Ultraviolet-Optical Telescope (UVOT; Roming et al. 2005) observed PKS 0537−441 in July (only *U*, *B*, and *V* filters) and 2005 November (all filters) simultaneously with the XRT. The log of the observations is reported in Table 2. UVOT data were taken also in 2004 December and 2005 January, but due to early orbit checkout and calibration, they are not reliable, and therefore we have not used them. The data analysis was performed using the `uvotsource` task included in the latest Heasoft software (see § 2.1.2). We subtracted the background and corrected for the coincidence loss effect (similar to the pileup for the XRT) in the case of a bright source. The magnitudes were converted into fluxes using the latest in-flight flux calibration factors and zero points.

REM acquired photometry of the AGN from 2004 December to 2005 March, and also in 2005 July and November, with various
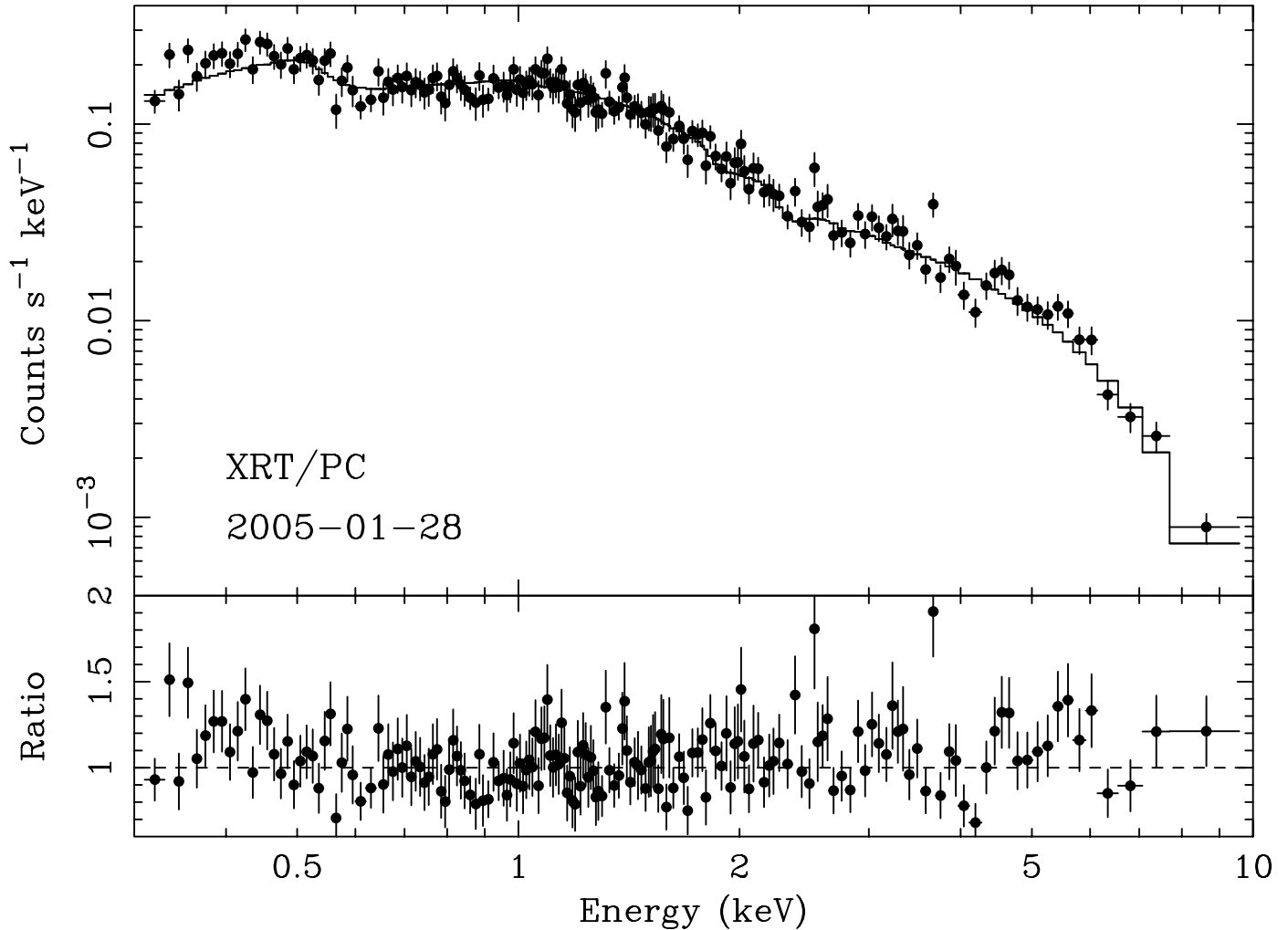
Fig. 1.—Observed *Swift* XRT spectrum taken on 2005 January 28. The solid stepped curve represents the single absorbed power law that best fits the spectrum (see Table 1 for spectral parameters).

combinations of filters. The data reduction followed standard procedures (see Dolcini et al. 2005). The log of the 2005 July and November observations is reported in Table 2, while the details of the previous REM observations have been presented in Dolcini et al. (2005).

## 3. RESULTS

### 3.1. *Multiwavelength Light Curves*

With a total *Swift* XRT exposure of 67 ks, PKS 0537−441 is one of the blazars best monitored by this instrument. Figure 2 shows the observed (i.e., not corrected for Galactic absorption), background-subtracted light curves extracted in the 0.2−1 and 1−10 keV energy bands. For direct comparison with the X-rays, the merged UVOT and REM light curve in the *V* band (covered by both instruments) is also shown in Figure 2. The UVOT *V*-band fluxes have been reduced to the central wavelength of the REM *V*-band observations using the power law $F_\nu \propto \nu^{-\beta}$, which best fits the optical spectrum in 2005 July ($\beta = 1.84 \pm 0.04$) and November ($\beta = 1.26 \pm 0.05$). The full transformation equation is $F_{\mathrm{UVOT},\,5505\,\text{Å}} = (5505/5460)^\beta \times F_{0,\,\mathrm{UVOT}-V} \times 10^{-0.4 V_{\mathrm{UVOT}}}$, where $F_{0,\,\mathrm{UVOT}-V}$ is the flux corresponding to zero UVOT *V* magnitude (equal to $3.19 \times 10^{-9}$ and $3.17 \times 10^{-9}$ ergs s$^{-1}$ cm$^{-2}$ Å$^{-1}$ for the 2005 July and November measurements, respectively). The REM and UVOT *V*-band data taken closest in time (2005 July

12) differ by ∼13%, the REM flux being lower than the UVOT flux. This difference may be intrinsic, since the REM and UVOT observations are about 6–7 hr apart; however, it is within the sum of the statistical uncertainties (see Table 2) and the systematic errors due to flux transformation and calibration of the two instruments (estimated to be no less than ∼5% altogether).

The optical *V*-band and X-ray light curves are highly correlated; however, the *V*-band flux varies with much higher amplitude. To the initial factor of 60 optical variation detected with REM between end of 2004 December and early 2005 February—noted and discussed in Dolcini et al. (2005)—corresponds a variation of only a factor of ∼2 of both soft (0.2–1 keV) and hard (1–10 keV) X-ray flux (Fig. 2). Thereafter, the flux decays nearly monotonically up to 2005 November both in optical and X-rays, with overall amplitudes of factors of ∼60 and ∼4, respectively. The variability indices of the X-ray light curves, defined as the ratios between the flux standard deviation around the mean flux and the mean flux itself ($\sigma/\langle f \rangle$), are 0.375 and 0.423 for the hard and soft X-rays, respectively, consistently lower than the optical variability index, 1.434 (the variability indices have been computed from the original data sets, i.e., before applying the temporal binning adopted in Fig. 2). The time behavior of the hardness ratio between the bands 0.2–1 and 1–10 keV shows no clear long-term trend: the spectrum hardens up to summer 2005 and softens thereafter, but only with marginal significance (Fig. 3*a*).

TABLE 2—Continued

TABLE 2

*Swift* UVOT and REM Observations of PKS 0537-441
in 2005 July and November

| Date (UT) | MJD[a] | Magnitude[b] |
|---|---|---|
| **UVOT UVW2 Filter (1930 Å)** | | |
| 2005 Nov: | | |
| 24.9243.................. | 53,698.9243 | 17.02 ± 0.04[c] |
| 24.9958.................. | 53,698.9958 | 16.86 ± 0.04 |
| 25.0646.................. | 53,699.0646 | 17.00 ± 0.05 |
| 25.2042.................. | 53,699.2042 | 16.91 ± 0.07 |
| 25.3313.................. | 53,699.3313 | 16.95 ± 0.05 |
| 25.3979.................. | 53,699.3979 | 17.03 ± 0.05 |
| 25.4653.................. | 53,699.4653 | 16.98 ± 0.05 |
| **UVOT UVM2 Filter (2200 Å)** | | |
| 2005 Nov: | | |
| 24.9312.................. | 53,698.9312 | 16.77 ± 0.05 |
| 25.0007.................. | 53,699.0007 | 16.88 ± 0.06 |
| 25.0688.................. | 53,699.0688 | 16.64 ± 0.06 |
| 25.1382.................. | 53,699.1382 | 16.60 ± 0.08 |
| 25.2063.................. | 53,699.2063 | 16.59 ± 0.09 |
| 25.3361.................. | 53,699.3361 | 16.89 ± 0.07 |
| 25.4028.................. | 53,699.4028 | 16.76 ± 0.06 |
| 25.4701.................. | 53,699.4701 | 16.73 ± 0.06 |
| **UVOT UVW1 Filter (2600 Å)** | | |
| 2005 Nov: | | |
| 24.9354.................. | 53,698.9354 | 16.60 ± 0.05 |
| 25.0035.................. | 53,699.0035 | 16.53 ± 0.06 |
| 25.0715.................. | 53,699.0715 | 16.70 ± 0.07 |
| 25.1396.................. | 53,699.1396 | 16.66 ± 0.10 |
| 25.2076.................. | 53,699.2076 | 16.62 ± 0.10 |
| 25.3389.................. | 53,699.3389 | 16.40 ± 0.06 |
| 25.4056.................. | 53,699.4056 | 16.67 ± 0.06 |
| 25.4729.................. | 53,699.4729 | 16.51 ± 0.06 |
| **UVOT U Filter (3450 Å)** | | |
| 2005 Jul: | | |
| 12.0530.................. | 53563.0530 | 14.05 ± 0.16 |
| 12.1190.................. | 53563.1190 | 14.03 ± 0.16 |
| 2005 Nov: | | |
| 17.0368.................. | 53,691.0368 | 16.22 ± 0.03 |
| 17.1042.................. | 53,691.1042 | 16.27 ± 0.03 |
| 17.1736.................. | 53,691.1736 | 16.24 ± 0.05 |
| 17.2201.................. | 53,691.2201 | 16.33 ± 0.06 |
| 17.2424.................. | 53,691.2424 | 16.16 ± 0.16 |
| 17.2896.................. | 53,691.2896 | 16.15 ± 0.03 |
| 17.3590.................. | 53,691.3590 | 16.16 ± 0.03 |
| 17.4264.................. | 53,691.4264 | 16.19 ± 0.02 |
| 17.4986.................. | 53,691.4986 | 16.22 ± 0.02 |
| 24.9375.................. | 53,698.9375 | 16.49 ± 0.05 |
| 25.0056.................. | 53,699.0056 | 16.56 ± 0.06 |
| 25.0736.................. | 53,699.0736 | 16.37 ± 0.06 |
| 25.1409.................. | 53,699.1409 | 16.50 ± 0.09 |
| 25.2083.................. | 53,699.2083 | 16.62 ± 0.10 |
| 25.3409.................. | 53,699.3409 | 16.57 ± 0.06 |
| 25.4076.................. | 53,699.4076 | 16.60 ± 0.06 |
| 25.4743.................. | 53,699.4743 | 16.63 ± 0.06 |
| **UVOT B Filter (4350 Å)** | | |
| 2005 Jul: | | |
| 12.0560.................. | 53563.0560 | 14.81 ± 0.08 |
| 12.1220.................. | 53563.1220 | 14.76 ± 0.08 |

| Date (UT) | MJD[a] | Magnitude[b] |
|---|---|---|
| **UVOT B Filter (4350 Å)** | | |
| 2005 Nov: | | |
| 17.0403.................. | 53,691.0403 | 16.97 ± 0.03 |
| 17.1076.................. | 53,691.1076 | 16.99 ± 0.04 |
| 17.1750.................. | 53,691.1750 | 17.03 ± 0.07 |
| 17.2208.................. | 53,691.2208 | 17.00 ± 0.07 |
| 17.2917.................. | 53,691.2917 | 17.03 ± 0.04 |
| 17.3625.................. | 53,691.3625 | 16.99 ± 0.03 |
| 17.4306.................. | 53,691.4306 | 16.97 ± 0.03 |
| 17.5056.................. | 53,691.5056 | 16.97 ± 0.02 |
| 24.9389.................. | 53,698.9389 | 17.36 ± 0.06 |
| 25.0069.................. | 53,699.0069 | 17.31 ± 0.08 |
| 25.0743.................. | 53,699.0743 | 17.37 ± 0.10 |
| 25.1409.................. | 53,699.1409 | 17.25 ± 0.14 |
| 25.3417.................. | 53,699.3417 | 17.34 ± 0.08 |
| 25.4090.................. | 53,699.4090 | 17.31 ± 0.08 |
| 25.4757.................. | 53,699.4757 | 17.22 ± 0.08 |
| **UVOT V Filter (5460 Å)** | | |
| 2005 Jul: | | |
| 12.0500.................. | 53563.0500 | 14.32 ± 0.09 |
| 12.1150.................. | 53563.1150 | 14.25 ± 0.09 |
| 2005 Nov: | | |
| 17.0340.................. | 53,691.0340 | 16.47 ± 0.04 |
| 17.1014.................. | 53,691.1014 | 16.39 ± 0.04 |
| 17.1729.................. | 53,691.1729 | 16.46 ± 0.07 |
| 17.2194.................. | 53,691.2194 | 16.58 ± 0.15 |
| 17.2424.................. | 53,691.2424 | 16.36 ± 0.21 |
| 17.2875.................. | 53,691.2875 | 16.48 ± 0.05 |
| 17.3556.................. | 53,691.3556 | 16.44 ± 0.04 |
| 17.4222.................. | 53,691.4222 | 16.43 ± 0.04 |
| 17.4910.................. | 53,691.4910 | 16.42 ± 0.03 |
| 24.9286.................. | 53,698.9286 | 16.81 ± 0.04 |
| 25.0000.................. | 53,699.0000 | 16.82 ± 0.09 |
| 25.0681.................. | 53,699.0681 | 16.88 ± 0.10 |
| 25.1382.................. | 53,699.1382 | 16.72 ± 0.13 |
| 25.2055.................. | 53,699.2055 | 16.85 ± 0.15 |
| 25.3354.................. | 53,699.3354 | 16.84 ± 0.10 |
| 25.4021.................. | 53,699.4021 | 16.89 ± 0.10 |
| 25.4694.................. | 53,699.4694 | 17.02 ± 0.11 |
| **REM V Filter (5505 Å)** | | |
| 2005 Jul: | | |
| 7.4375.................... | 53558.4375 | 15.72 ± 0.03 |
| 9.4219.................... | 53560.4219 | 15.21 ± 0.02 |
| 10.4336.................. | 53561.4336 | 14.80 ± 0.02 |
| 11.4297.................. | 53562.4297 | 14.40 ± 0.02 |
| 12.4297.................. | 53563.4297 | 14.52 ± 0.02 |
| 12.4375.................. | 53563.4375 | 14.47 ± 0.02 |
| 12.4414.................. | 53563.4414 | 14.50 ± 0.02 |
| 22.3984.................. | 53573.3984 | 15.47 ± 0.04 |
| 22.4336.................. | 53573.4336 | 15.73 ± 0.03 |
| 2005 Nov: | | |
| 7.2494.................... | 53,681.2494 | 16.93 ± 0.11 |
| 19.2346.................. | 53,693.2346 | 17.07 ± 0.13 |
| 20.2174.................. | 53,694.2174 | 17.17 ± 0.14 |
| 30.2021.................. | 53704.2021 | 17.46 ± 0.17 |
| **REM R Filter (6588 Å)** | | |
| 2005 Jul: | | |
| 7.4375.................... | 53558.4375 | 15.06 ± 0.01 |
| 9.4219.................... | 53560.4219 | 14.56 ± 0.01 |

TABLE 2—Continued

| Date (UT) | MJD[a] | Magnitude[b] |
|---|---|---|
| REM R Filter (6588 Å) | | |
| 11.4336.................. | 53562.4336 | 13.75 ± 0.04 |
| 12.4258.................. | 53563.4258 | 13.91 ± 0.01 |
| 12.4297.................. | 53563.4297 | 13.91 ± 0.01 |
| 12.4375.................. | 53563.4375 | 13.87 ± 0.01 |
| 13.4414.................. | 53564.4414 | 14.04 ± 0.06 |
| 22.4023.................. | 53573.4023 | 14.87 ± 0.02 |
| 2005 Nov: | | |
| 6.2533.................... | 53,680.2533 | 16.39 ± 0.07 |
| 7.2522.................... | 53,681.2522 | 16.39 ± 0.04 |
| 18.2249.................. | 53,692.2249 | 16.41 ± 0.06 |
| 19.2452.................. | 53,693.2452 | 16.20 ± 0.06 |
| 20.2280.................. | 53,694.2280 | 16.35 ± 0.07 |
| 30.2127.................. | 53704.2127 | 16.92 ± 0.08 |
| REM I Filter (8060 Å) | | |
| 2005 Jul: | | |
| 7.4375.................... | 53558.4375 | 14.40 ± 0.01 |
| 9.4219.................... | 53560.4219 | 13.91 ± 0.01 |
| 10.4375.................. | 53561.4375 | 13.48 ± 0.01 |
| 11.4336.................. | 53562.4336 | 13.14 ± 0.03 |
| 12.4258.................. | 53563.4258 | 13.26 ± 0.01 |
| 12.4336.................. | 53563.4336 | 13.23 ± 0.01 |
| 12.4414.................. | 53563.4414 | 13.24 ± 0.01 |
| 20.4414.................. | 53571.4414 | 13.82 ± 0.03 |
| 22.4062.................. | 53573.4062 | 14.13 ± 0.02 |
| 22.4375.................. | 53573.4375 | 14.22 ± 0.02 |
| 2005 Nov: | | |
| 6.2559.................... | 53,680.2559 | 15.60 ± 0.08 |
| 7.2549.................... | 53,681.2549 | 15.78 ± 0.07 |
| 18.2355.................. | 53,692.2355 | 15.82 ± 0.08 |
| 19.2560.................. | 53,693.2560 | 15.72 ± 0.07 |
| 20.2386.................. | 53,694.2386 | 15.89 ± 0.10 |
| 30.2235.................. | 53704.2235 | 16.23 ± 0.09 |
| REM H Filter (16000 Å) | | |
| 2005 Nov: | | |
| 2.1718.................... | 53,676.1718 | 12.77 ± 0.07 |
| 2.1738.................... | 53,676.1738 | 12.89 ± 0.08 |
| 2.1759.................... | 53,676.1759 | 12.93 ± 0.08 |
| 2.1805.................... | 53,676.1805 | 12.89 ± 0.10 |
| 2.1820.................... | 53,676.1820 | 12.70 ± 0.06 |
| 2.1917.................... | 53,676.1917 | 12.80 ± 0.07 |
| 2.1941.................... | 53,676.1941 | 12.75 ± 0.07 |
| 2.1962.................... | 53,676.1962 | 12.85 ± 0.07 |
| 2.2003.................... | 53,676.2003 | 12.77 ± 0.08 |
| 2.2895.................... | 53,676.2895 | 12.75 ± 0.07 |
| 2.2957.................... | 53,676.2957 | 13.05 ± 0.06 |
| 2.3027.................... | 53,676.3027 | 12.88 ± 0.08 |
| 2.3048.................... | 53,676.3048 | 12.78 ± 0.07 |
| 2.3068.................... | 53,676.3068 | 12.73 ± 0.06 |
| 2.3089.................... | 53,676.3089 | 12.96 ± 0.08 |
| 3.2822.................... | 53,677.2822 | 12.95 ± 0.07 |
| 3.2864.................... | 53,677.2864 | 12.78 ± 0.06 |
| 3.2885.................... | 53,677.2885 | 12.83 ± 0.07 |
| 3.2905.................... | 53,677.2905 | 12.72 ± 0.06 |
| 3.2929.................... | 53,677.2929 | 12.66 ± 0.06 |
| 3.2950.................... | 53,677.2950 | 12.91 ± 0.09 |
| 3.3006.................... | 53,677.3006 | 12.78 ± 0.07 |
| 3.3027.................... | 53,677.3027 | 12.70 ± 0.08 |
| 3.3047.................... | 53,677.3047 | 12.63 ± 0.07 |
| 3.3068.................... | 53,677.3068 | 12.80 ± 0.07 |
| 3.3088.................... | 53,677.3088 | 12.67 ± 0.06 |
| 3.3112.................... | 53,677.3112 | 12.90 ± 0.08 |

TABLE 2—Continued

| Date (UT) | MJD[a] | Magnitude[b] |
|---|---|---|
| REM H Filter (16000 Å) | | |
| 3.3133.................... | 53,677.3133 | 12.98 ± 0.07 |
| 3.3154.................... | 53,677.3154 | 12.84 ± 0.07 |
| 3.3174.................... | 53,677.3174 | 12.98 ± 0.07 |
| 3.3195.................... | 53,677.3195 | 12.95 ± 0.07 |
| 3.3219.................... | 53,677.3219 | 13.08 ± 0.07 |
| 3.3240.................... | 53,677.3240 | 12.75 ± 0.07 |
| 3.3260.................... | 53,677.3260 | 12.79 ± 0.06 |
| 3.3281.................... | 53,677.3281 | 12.74 ± 0.06 |
| 3.3302.................... | 53,677.3302 | 12.84 ± 0.08 |
| 17.1083.................. | 53,691.1083 | 12.42 ± 0.08 |
| 18.2154.................. | 53,692.2154 | 12.68 ± 0.06 |
| 18.2208.................. | 53,692.2208 | 12.64 ± 0.07 |
| 18.2229.................. | 53,692.2229 | 12.61 ± 0.08 |
| 18.2249.................. | 53,692.2249 | 12.70 ± 0.07 |
| 2005 Nov: | | |
| 18.2273.................. | 53,692.2273 | 12.64 ± 0.06 |
| 18.2296.................. | 53,692.2296 | 12.63 ± 0.07 |
| 18.2314.................. | 53,692.2314 | 12.74 ± 0.06 |
| 18.2335.................. | 53,692.2335 | 12.73 ± 0.07 |
| 18.2355.................. | 53,692.2355 | 12.61 ± 0.06 |
| 18.2379.................. | 53,692.2379 | 12.71 ± 0.07 |
| 18.2399.................. | 53,692.2399 | 12.51 ± 0.06 |
| 18.2420.................. | 53,692.2420 | 12.61 ± 0.07 |
| 18.2440.................. | 53,692.2440 | 12.70 ± 0.06 |
| 18.2461.................. | 53,692.2461 | 12.60 ± 0.07 |
| 18.2626.................. | 53,692.2626 | 12.68 ± 0.07 |
| 18.2654.................. | 53,692.2654 | 12.68 ± 0.07 |
| 18.2688.................. | 53,692.2688 | 12.62 ± 0.07 |
| 19.2350.................. | 53,693.2350 | 12.65 ± 0.07 |
| 19.2371.................. | 53,693.2371 | 12.54 ± 0.08 |
| 19.2391.................. | 53,693.2391 | 12.72 ± 0.08 |
| 19.2412.................. | 53,693.2412 | 12.65 ± 0.08 |
| 19.2432.................. | 53,693.2432 | 12.55 ± 0.07 |
| 19.2453.................. | 53,693.2453 | 12.59 ± 0.07 |
| 19.2476.................. | 53,693.2476 | 12.52 ± 0.07 |
| 19.2497.................. | 53,693.2497 | 12.54 ± 0.08 |
| 19.2518.................. | 53,693.2518 | 12.66 ± 0.07 |
| 19.2605.................. | 53,693.2605 | 12.54 ± 0.06 |
| 20.2220.................. | 53,694.2220 | 12.74 ± 0.07 |
| 20.2240.................. | 53,694.2240 | 12.96 ± 0.07 |
| 20.2249.................. | 53,694.2249 | 12.66 ± 0.06 |
| 20.2261.................. | 53,694.2261 | 12.83 ± 0.07 |
| 20.2281.................. | 53,694.2281 | 12.83 ± 0.06 |
| 20.2346.................. | 53,694.2346 | 12.77 ± 0.06 |
| 20.2366.................. | 53,694.2366 | 12.62 ± 0.05 |
| 20.2387.................. | 53,694.2387 | 12.76 ± 0.06 |
| 20.2411.................. | 53,694.2411 | 12.74 ± 0.06 |
| 20.2431.................. | 53,694.2431 | 12.85 ± 0.07 |
| 20.2452.................. | 53,694.2452 | 12.77 ± 0.07 |
| 20.2472.................. | 53,694.2472 | 12.82 ± 0.07 |
| 20.2493.................. | 53,694.2493 | 12.66 ± 0.06 |
| 20.2513.................. | 53,694.2513 | 12.74 ± 0.07 |
| 30.1977.................. | 53,704.1977 | 13.10 ± 0.08 |
| 30.2115.................. | 53,704.2115 | 13.20 ± 0.10 |
| 30.2135.................. | 53,704.2135 | 13.33 ± 0.11 |
| 30.2179.................. | 53,704.2179 | 13.37 ± 0.10 |
| 30.2200.................. | 53,704.2200 | 13.08 ± 0.10 |
| 30.2371.................. | 53,704.2371 | 13.20 ± 0.10 |

Note.—Typical exposure times are 4–5 minutes, both for UVOT and REM.
[a] Modified Julian Date. We used the convention MJD = JD − 2, 400, 000.5.
[b] Not corrected for Galactic extinction.
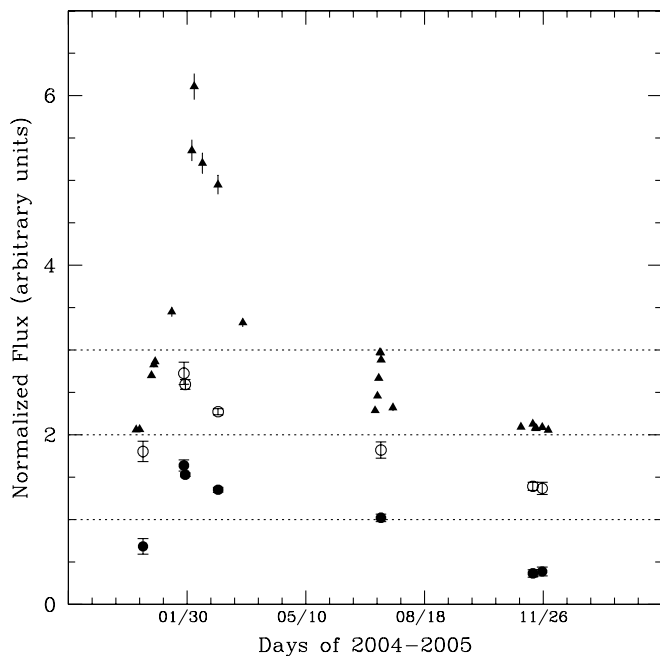[c] Errors represent 1 $\sigma$ statistical uncertainties.

FIG. 2.—*Swift* XRT background-subtracted light curves in the 1−10 keV (*filled circles*) and 0.2−1 keV (*open circles*) energy bands, and optical light curve (*triangles*), obtained from the merging of the UVOT *V* filter and REM *V* filter observations. The signal has been averaged within the *Swift* pointings for the X-ray data and with a time resolution of 1 day for the optical data. The curves are not corrected for Galactic extinction, and are normalized to their respective averages (0.136 counts s$^{-1}$ in the 1−10 keV band, 0.084 counts s$^{-1}$ in the 0.2−1 keV band, 6.58 mJy in the optical band), computed on the time-binned data sets. The dotted horizontal lines indicate the average values of the three light curves: for clarity, the 0.2−1 keV band and *V*-band light curves have been scaled up by additive constants 1 and 2, respectively. Note that this upscaling implies that the flux ratios derived by direct inspection of the soft X-ray (0.2−1 keV) and optical light curves do not correspond to the real ones, the fluxes having been increased by constants 1 and 2, respectively. The maximum amplitudes of variability in optical and X-rays are a factor of ∼4 and ∼60, respectively.

In Figure 4 portions of the light curves are reported in smaller time intervals. The X-ray flux presents an almost fully resolved flare on 2005 January 27−28 with somewhat higher total amplitude in the soft than in the hard band (factors of ∼2 and ∼1.5, respectively, see Figs. 3*b* and 4*a*). The correlated optical and X-ray behavior on short timescales (days to hours) has no precise character: while the limited simultaneous X-ray and optical sampling in 2005 July shows a well-correlated decay in the 2 bands, with the X-ray flux declining faster than the optical flux (Fig. 4*b*), the factor of 2 X-ray variations in 2005 November have no counterpart in UV-optical, where flickering of at most ∼10% is observed (Figs. 4*c* and 4*d*).

Obviously, the better long-term sampling available at optical wavelengths favors the detection of day timescale variations in optical with respect to the X-rays. This is relevant when attempting to determine a possible time lag between the optical and X-ray light curves. While we can constrain the occurrence of the optical maximum (formally observed on 2005 February 5) within the time window 2005 February 3−12, the X-ray light curve maximum is much less well constrained. Figure 4*a* indicates that the X-ray observed maximum occurred between 2005 January 27 and 28. If this is the absolute peak of the X-ray light curve, and it is correlated with that in the optical, then it has preceded the optical maximum by at least 1 week in the observer frame. However, given the sampling of the X-ray light curve, we cannot exclude more intense and unobserved flares preceding or following the observed X-ray maximum by time intervals of up to ∼1 month.
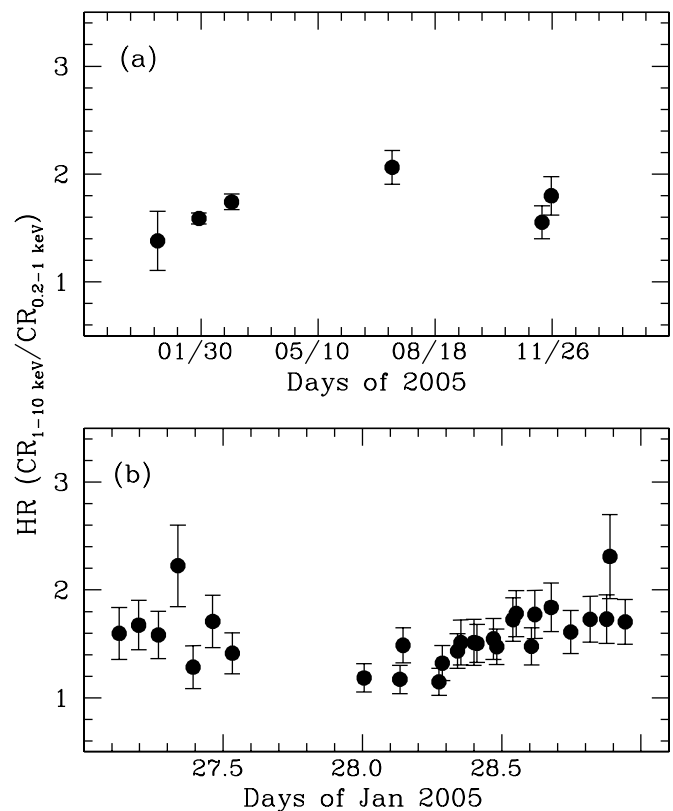


FIG. 3.—Hardness ratios computed using the 1−10 and 0.2−1 keV count rates for (*a*) the whole monitoring; (*b*) the observation of 2005 January.

Therefore, this is our upper limit on the time lag of the correlation between the X-ray and optical light curves.

### 3.2. *Broadband Spectrum*

In Figure 5 we report the broadband spectral energy distributions of PKS 0537−441 at three epochs during our *Swift* and REM campaign, representative of three different emission states: 2005 February 24−25, 2005 July 12, and 2005 November 24 for the bright, intermediate, and low states, respectively. The spectral energy distribution of 2005 November 24 has been selected because the *Swift* UVOT observations made on that day cover the near-UV wavelengths (1930−2600 Å), unlike those of 17 November, that are limited to the *UBV* filters (Table 2). However, no strictly simultaneous REM data are available on 24 November. The REM data of 2005 November 20 and 30 have been used instead, and interpolated at the date of 24 November. We exclude that possible variability between 2005 November 20 and 30 may significantly affect the reliability of the REM fluxes obtained through interpolation: no large variability is observed in this period (see Table 2); the UVOT and REM *V*-band points are consistent (see Fig. 5); we have verified that the shape of the near-IR to near-UV spectrum of 2005 November 24 is similar to that of 2005 November 17 (constructed with data simultaneous within 1 day), in the common wavelength range (3400−16000 Å).

Whenever more than one UVOT or REM measurement is available at a given date and filter, we take the flux average. The associated error is the standard deviation when three or more data points are averaged. When only two measurements are available, the error is the larger of the two individual errors, or the flux difference, whichever is larger. The X-ray data are corrected for photoelectric absorption by the Galactic neutral hydrogen as described in § 2.1.2, and the near-infrared to ultraviolet data are corrected for Galactic dust absorption with $E(B-V) = 0.037$
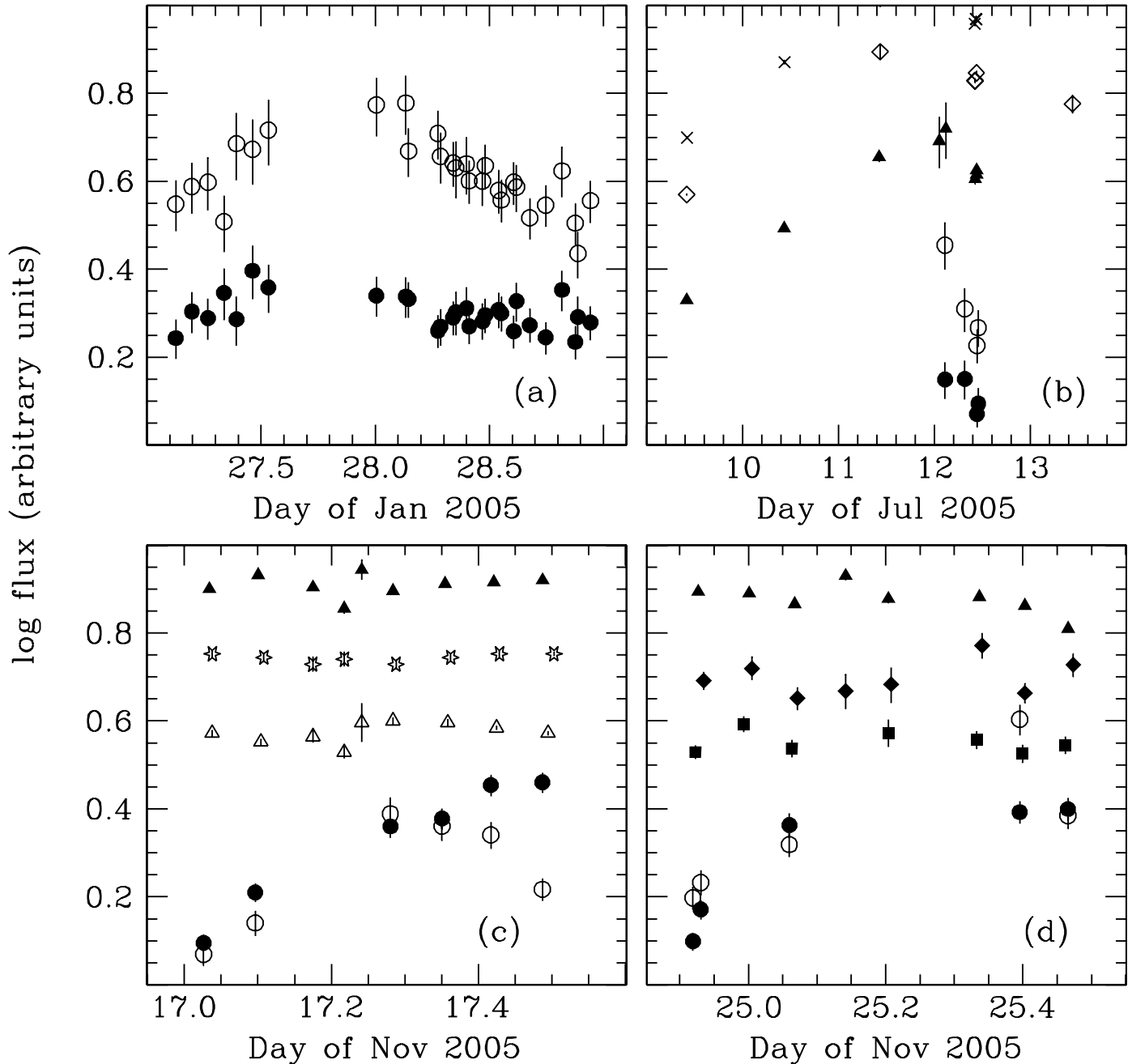
Fig. 4.—Multiwavelength light curves at various epochs during the 2005 campaign, in logarithmic scale, shifted in flux by arbitrary additive constants: (*a*) 1–10 keV (*filled circles*) and 0.2–1 keV (*open circles*) XRT light curves in 2005 January; (*b*) XRT light curves in 2005 July (symbols as in panel *a*), and simultaneous REM and UVOT *V*-band (*filled triangles*), REM *R*- (*open diamonds*), and *I*-band (*crosses*) light curves. Note the optical increase preceding the X-ray observation and the correlated X-ray and optical decay; (*c*) XRT light curves on 2005 November 17 (symbols as in panel *a*), and UVOT *U*- (*open triangles*), *B*- (*stars*), and *V*-band (*filled triangles*) light curves; (*d*) XRT light curves in 2005 November 24–25 (symbols as in panel *a*), and UVOT light curves in the W2 (1930 Å; *filled squares*), W1 (2600 Å; *filled diamonds*), and *V* filters (*filled triangles*).

(Schlegel et al. 1998), using the extinction law of Cardelli et al. (1989). For comparison, we have reported also the historical multi-wavelength spectra obtained in 1991–1992 and 1995 (see Pian et al. 2002) and the nonsimultaneous *IRAS, ISO, HST*, and *BeppoSAX* data taken at various epochs (Padovani et al. 2006; Pian et al. 2002).

The 2005 optical spectra, spanning a factor of ∼50 in normalization, bracket the historical optical observations. They are described by single power laws and are steeper at higher states. The near-IR flux varies with lower amplitude. At the lowest state of November 2005, we note a large discrepancy between the optical

and infrared fluxes: the *H*-band flux exceeds by a factor of ∼4 the extrapolation of the optical spectrum to the *H*-band wavelengths. The flatness of the November optical–UV spectrum and the spectral discontinuity between the optical and near-IR wave bands suggest that in the lower states different emission components play a role in shaping the spectrum. In particular, radiation produced by the accretion disk may partially account for the optical–UV spectrum. This behavior is reminiscent of that seen in 3C 279 (Pian et al. 1999).

The X-ray fluxes detected by XRT encompass both the *BeppoSAX* and *ROSAT* states. The steadiness of the XRT spectral
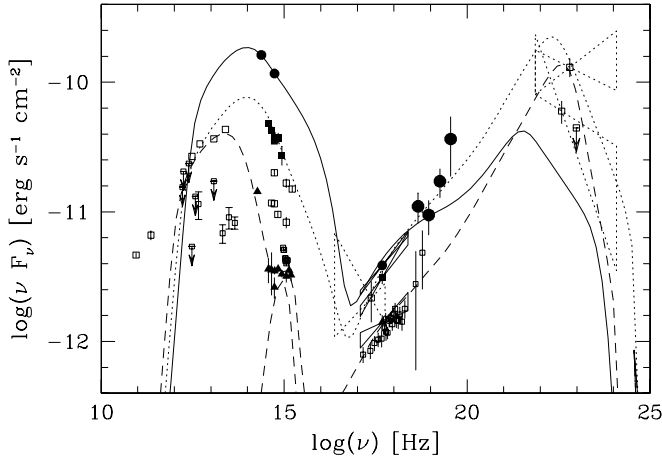
Fig. 5.—Observed spectral energy distributions of PKS 0537−441 on 2005 February 24–25 (*small filled circles*), 2005 July 12 (*filled squares*), and 2005 November 24 (*filled triangles*). The big filled circles represent the BAT data. The *Swift* XRT data are reported along with the 1 σ confidence ranges of their power-law fits. Systematic errors of 5% and 10% have been added in quadrature to the statistical uncertainties associated with the UVOT UBV filters and UV filters data points, respectively. For comparison, in lighter, open squares the multiwavelength data from previous epochs are reported (including *CGRO* EGRET spectra), already discussed in Pian et al. (2002), and the nonsimultaneous *IRAS, ISO, HST* FOS, and *BeppoSAX* data (Pian et al. 2002; Padovani et al. 2006). The 1 σ confidence ranges of the EGRET spectra are reported as light dashed lines. The flux uncertainties are 1 σ (in some cases they are smaller than the symbol size). The X-ray, UV, optical, and near-IR data are corrected for Galactic extinction (see text). The optical and near-IR magnitudes have been converted to fluxes following Fukugita et al. (1995) and Bersanelli et al. (1991), respectively. Overplotted are the jet models (Katarzyński & Ghisellini 2007, see text) for the energy distributions of 2005 February 24–25 (*solid curve*), 2005 July 12 (*dotted curve*), 2005 November 24 (*dashed curve*). The thermal component required to account for the observed optical–UV flux is also reported as a dashed curve.

slope over time, as opposed to a factor of 4 variation in the normalization, is remarkable. The X-ray spectral shape is also very similar to that of the *BeppoSAX* spectrum, which covers an energy range similar to that covered by XRT.

The BAT spectrum is dominated by the episodes of more intense activity of 2005 January–February and July, and despite its large uncertainty gives a good estimate of the spectral shape at hard X-rays in high state.

## 4. DISCUSSION

The character of the multiwavelength variability detected by our monitoring is extremely unusual: the outburst of PKS 0537−441, jointly monitored by XRT and REM from its rise in 2004 December–2005 January though its long decay, which ended in 2005 November, has a remarkably higher amplitude at optical (factor of ∼60) than at X-ray frequencies (factor of ∼4). These obviously represent only lower limits to the variability, the intrinsic amplitude of which may be contaminated by a constant component that is more relevant in X-rays than in the optical. The optical spectra suggest the presence of an underlying thermal optical component in low state (§ 3.2), presumably only modestly variable. However, trying to assess whether—and how significantly—this dilutes the intrinsic multiwavelength variability of the nonthermal flux is prone to many uncertainties. The sampling of our monitoring indicates that the long-term decay is monotonic (Fig. 2), but small flares are present on day timescales (Fig. 4).

The fact that the optical–UV flux variability has a much larger amplitude than the simultaneous X–ray flux variability may at first sight be surprising. In a simple synchrotron self-Compton scenario, where the optical emission is due to synchrotron ra-

diation and the X-rays are due to inverse Compton scattering off the synchrotron photons, one would expect to observe the opposite if the changing parameter is the density of the emitting particles. In fact, the self-Compton emissivity scales with the square of the particle density, while the synchrotron emissivity varies linearly with it. If instead the varying parameter is the magnetic field, we expect that both the synchrotron and the synchrotron self-Compton fluxes vary with the same amplitude.

On the other hand, in models producing the high-energy emission by up-scattering of radiation produced outside the jet ("external" Compton), both the synchrotron and the inverse Compton fluxes vary linearly with the particle density. In these models, a variation of the magnetic field could produce a variation of the synchrotron flux leaving almost unchanged the inverse Compton flux.

Note also that the X-ray and optical spectra in these models derive from very different portions of the relativistic electron distribution: the optical emission originates from electrons above the spectral break, while the X-rays are produced via inverse Compton scattering of synchrotron or external photons by electrons of much lower energies.

We applied a simple, one-zone, homogeneous synchrotron self-Compton plus external inverse Compton model to the different states of PKS 0537−441. The model is described in Ghisellini et al. (2002). The general assumptions are the following:

1. The source is a cylinder of cross sectional radius $R = \psi z$, where $z$ is the distance from the apex of the jet, assumed to be a cone of semiaperture angle $\psi$. The width $\Delta R'$, as measured in the comoving frame, is assumed to be equal to $R$.

2. The magnetic field $B$ is homogeneous and tangled.

3. The blob moves with a bulk Lorentz factor, $\Gamma$ and the viewing angle is $\theta$ (we assumed here $\theta = 3°$).

4. The external radiation is produced at a fixed radius, which can be identified with the radius of the broad-line region. We assume that 10% of the disk luminosity is reprocessed by the broad-line region. These assumptions should be taken with care, because, beside the contribution of the broad-line region, other processes can contribute to the external radiation (scattering by ionized intercloud plasma, synchrotron radiation "mirrored" by the clouds and/or the walls of the jet, reprocessing by a molecular torus [Sikora et al. 1994; Błażejowski et al. 2000; Ghisellini & Madau 1996], and finally, direct radiation from the accretion disk [Dermer & Schlickeiser 1993; see also Celotti et al. 2007]).

5. The particle distribution is the result of injection and cooling. We calculate the random Lorentz factor $\gamma_{cool}$ at which the particles cool in one light crossing time. If the particles are injected between $\gamma_{inj}$ and $\gamma_{max}$ with a power-law distribution of slope $s$, in the "fast cooling" regime ($\gamma_{cool} < \gamma_{inj}$), we have an emitting particle distribution $N(\gamma) \propto \gamma^{-p}$ between $\gamma_{inj}$ and $\gamma_{max}$ (where $p = s + 1$ is the injection slope increased by one unit), and $N(\gamma) \propto \gamma^{-2}$ between $\gamma_{cool}$ and $\gamma_{inj}$ (Ghisellini et al. 1998, 2002; Ghisellini 1989). In the models presented here, this is always the case, since the adopted parameters (see Table 3) imply that the radiative cooling (synchrotron, synchrotron self-Compton, and external Compton) is fast, and guarantee that $\gamma_{cool}$ is always smaller than $\gamma_{inj}$ and close to unity (after a light crossing time).

Based on the above assumptions, the modeling of the spectral energy distribution yields the results shown in Figure 5, where we report model curves for three states of the source during our 2005 campaign. We have also modeled under similar assumptions previous multiwavelength energy distributions of PKS 0537−441, presented in Pian et al. (2002), including data in the MeV–GeV domain from *CGRO* EGRET (Fig. 6). The radiation processes at

TABLE 3
MODEL PARAMETERS

| Parameter | 2005 February | 2005 July | 2005 November | 1991–1992 | 1995 |
|---|---|---|---|---|---|
| $\Gamma$ | 10 | 12 | 15 | 15 | 15 |
| $R$ ($10^{15}$ cm) | 16 | 19 | 28 | 28 | 28 |
| $B$ [G] | 40 | 12 | 7 | 6 | 7 |
| $\gamma_b$ | 250 | 500 | 380 | 200 | 310 |
| $\gamma_{max}$ | $3e3$ | $6 \cdot e3$ | $2e4$ | $7e3$ | $2e4$ |
| $p$ | 3.8 | 4.4 | 6.2 | 3.5 | 4.2 |
| $L'_{inj}$ ($10^{45}$ ergs s$^{-1}$) | 0.095 | 0.07 | 0.025 | 0.045 | 0.03 |
| $\nu_{ext}$ ($10^{15}$ Hz) | 0.3 | 0.5 | 1.5 | 1.5 | 1.5 |
| $U_{ext}$ (ergs cm$^{-3}$) | 0.085 | 0.069 | 0.016 | 0.016 | 0.016 |
| $\delta$ | 15.7 | 17.2 | 18.6 | 18.6 | 18.6 |
| $L_B$ ($10^{45}$ ergs s$^{-1}$) | 253 | 28 | 32.3 | 23.8 | 32.3 |
| $L_p$ ($10^{45}$ ergs s$^{-1}$) | 24.5 | 42 | 53.2 | 96.8 | 46.6 |
| $L_e$ ($10^{45}$ ergs s$^{-1}$) | 0.08 | 0.18 | 0.29 | 0.51 | 0.25 |
| $L_{rad}$ [($10^{45}$ ergs s$^{-1}$) | 8.8 | 10.2 | 5.6 | 9.95 | 5.5 |

NOTES.—For all models we have assumed a viewing angle $\theta = 3°$ and a bolometric luminosity of the accretion disk $L_{disk} = 1.8 \times 10^{46}$ ergs s$^{-1}$. The energy density of the external radiation and its peak frequency $\nu_{ext}$ are measured in the observer frame.

work are synchrotron at radio-to-UV frequencies, and inverse Compton scattering off both synchrotron photons (self-Compton) and external photons, dominating at X-ray and gamma-ray frequencies, respectively. The input parameters used for these models are listed in the upper part of Table 3. In the lower part we report some interesting output parameters, namely the Doppler factor $\delta$ and the power carried by the jet in the form of magnetic field ($L_B$), cold protons ($L_p$), relativistic electrons ($L_e$), and produced radiation ($L_{rad}$), defined as

$$L_B = \pi R^2 \Gamma^2 c U_B,$$

$$L_p = \pi R^2 \Gamma^2 c \int N(\gamma) m_p c^2 \, d\gamma,$$

$$L_e = \pi R^2 \Gamma^2 c \int N(\gamma) \gamma m_e c^2 \, d\gamma,$$

$$L_{rad} = \pi R^2 \Gamma^2 c U'_{rad}, \qquad (1)$$

where $U_B$ and $U'_{rad}$ are the magnetic and the radiation energy density measured in the comoving frame, respectively.

Usually, when applying a single-zone synchrotron and inverse Compton model, the choice of the input parameters is not unique, especially when the peak of the inverse Compton component is not observed, as in our case. However, we were guided in our choice by the knowledge of the total luminosity of the broad lines ($\sim 5 \times 10^{44}$ ergs s$^{-1}$; Pian et al. 2005), and the requirement that the spectra observed here in the low optical–UV state are unusually flat because they are "contaminated" by the thermal accretion disk component. We can then infer the luminosity of this component (which we have fixed to $1.8 \times 10^{46}$ ergs s$^{-1}$). Note also that in the low state of 2005 November the flux in the $H$ filter suggests that the synchrotron spectrum on these occasions is very steep. The other requirements we have applied, which help us in choosing the input parameters, include minimizing the total power budget and describing the different states of the source with a minimal change of the power carried by the jet. The latter point is crucial, because it allows a direct test once high-energy observations—as will be performed by *GLAST*—will be available. In fact it is possible to obtain reasonably good fits by allowing the jet power to vary by a large amount from state to state, being larger in high states. This would however correspond to very different spectra and fluxes in the MeV–GeV band.

Remarkably, the chosen parameters correspond closely to the expectations of the jet radiation model proposed by Katarzyński & Ghisellini (2007): dramatic variations in specific frequency bands can be produced by relativistic jets carrying the same amount of energy in bulk relativistic and Poynting flux form. In fact, if blobs having the same bulk kinetic energy $\Gamma M c^2$ (where $M$ is the mass of the blob) dissipate a fraction of their kinetic energy at different locations along the jet, and if the distance of the emitting region from the origin of the jet is directly related to $\Gamma$, then slow blobs will dissipate closer to the jet apex, when the blob is more compact, and embedded in a larger magnetic field. In this case the external Compton scattering is reduced because the external radiation energy density as seen in the comoving frame ($\propto \Gamma^2$) is lower, while the synchrotron radiation ($\propto B^2$) is likely to be enhanced, since we expect larger values of the magnetic field closer to the apex of the jet.
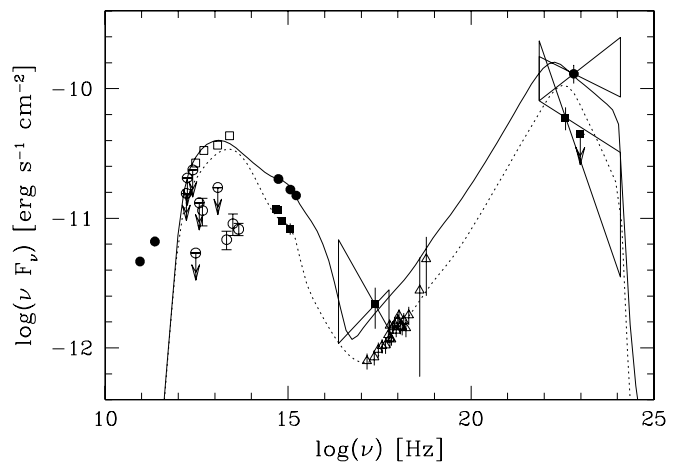


FIG. 6.—Historical spectral energy distributions of PKS 0537−441. The data are the same as those presented in Fig. 5 as open squares. Here we distinguish them according to the observation epoch: the gamma-ray (*CGRO* EGRET), soft X-ray (*ROSAT*), UV (*IUE*), optical, and millimetric data have been taken nearly simultaneously in 1991–1992 (*filled squares*) and 1995 (*filled circles*). The far-infrared data taken by *IRAS* and *ISO* and the X-ray *BeppoSAX* data are not simultaneous and are represented as open squares, open circles, and open triangles, respectively (see Pian et al. 2002 and references therein; Padovani et al. 2006). As in Fig. 5, the data have been modeled according to Katarzyński & Ghisellini (2007). The model curves for the 1991–1992 and 1995 states are shown by the dotted and solid lines, respectively.
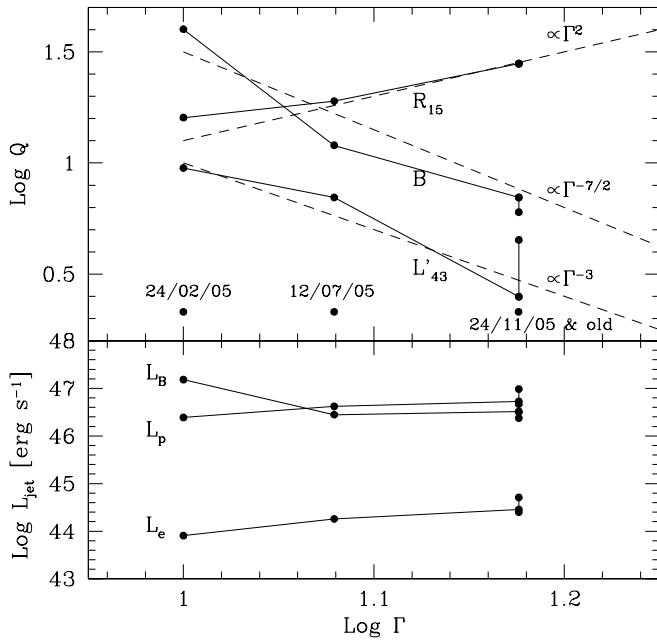
FIG. 7.—*Top panel:* The logarithms of three quantities ("$Q$") are reported as a function of the logarithm of the bulk Lorentz factor: the size of the emitting source $R_{15}$ in units of $10^{15}$ cm, the value of the magnetic field $B$ in Gauss, and the injected power $L'_{43}$ (in the comoving frame) in the form of relativistic particles, in units of $10^{43}$ ergs s$^{-1}$, as used for our modeling. The dashed lines represent the relationships predicted by the Katarzyński & Ghisellini (2007) model. The labeled dates identify the specific model/state of the source (see Table 3). *Bottom panel:* The power carried by the jet in the form of magnetic field ($L_B$), cold protons ($L_p$), relativistic electrons ($L_e$) resulting from our modeling, as a function of the bulk Lorentz factor. [*See the electronic edition of the Journal for a color version of this figure.*]

In this picture the key ingredient is the link between the dissipation site and the bulk Lorentz factor at that location: smaller Lorentz factors are required for smaller distances between the jet apex and the dissipation site. There are two scenarios: the blob could be still accelerating when it dissipates, or else the dissipation is the result of internal shocks. In Katarzyński & Ghisellini (2007) the second scenario is adopted, because it provides the scalings needed to characterize completely the model. In this scenario (see its specific application to blazars by Ghisellini [1999], Spada et al. [2001], and Guetta et al. [2004]), faster blobs can catch up with slower ones at a distance $z = \Gamma^2 \Delta z_0$ from the jet origin, where $z_0$ is the initial separation of the two blobs, and $\Delta$ is their thickness.

Furthermore, in the Katarzyński & Ghisellini (2007) model, it is assumed that the blobs always carry the same amount of bulk kinetic energy ($\Gamma Mc^2$ is the same) and magnetic energy ($\Gamma B^2 V'$ is the same, where $B$ and $V'$ are the magnetic field and volume measured in the comoving frame of the source, respectively). As a result of the dissipation process, the fraction of the available energy transferred to the emitting electrons is the same (i.e., the efficiency is the same). Based on these assumptions, we can assign for all the input parameters their scalings with $\Gamma$: therefore, when fitting two or more different states of the same source with this model, once we have chosen the parameters for one state we are left with only one free parameter, i.e., the bulk Lorentz factor $\Gamma$. We can relax this by allowing the particle distribution slopes to be changed, as well as the fraction of the electron population that is accelerated to relativistic energies. This does not violate any strong requirement.

In Figure 7 it is shown how the choice of the present input parameters compares with the Katarzyński & Ghisellini (2007) prescriptions, namely, $B \propto \Gamma^{-7/2}$, $R \propto \Gamma^2$ and $L'_{\rm inj} \propto \Gamma^{-3}$. We also show (*bottom panel*) that the power carried by the jet is almost constant. The good agreement leads us to conclude that the variations seen in this source are probably due to (*small*) variations in the bulk Lorentz factor, which induces dissipation to occur at different locations along the jet. Consequently, the emitting regions have different radii, particle densities and magnetic fields. Note that variations of $\Gamma$ between 10 and 15 can explain the entire observed variability. In this respect, PKS 0537−441 is very similar to 3C 454.3 during its large 2005 multiwavelength flare (Fuhrmann et al. 2006; Pian et al. 2006; Giommi et al. 2006). For that source, the 100-fold amplitude of the optical variability could be accounted for by changing $\Gamma$ by a factor of less than 2 (Katarzyński & Ghisellini 2007).

The knowledge of the spectrum of PKS 0537−441 at MeV–GeV energies is crucial for fully constraining the models. Therefore, PKS 0537−441 qualifies as a prime candidate for further monitoring with *Swift* and for simultaneous observations with *INTEGRAL*, AGILE, and *GLAST*.

REFERENCES

Aharonian, F., et al. 2006, A&A, 455, 461
Albert, J., et al. 2006, ApJ, 648, L105
Bersanelli, M., Bouchet, P., & Falomo, E. 1991, A&A, 252, 854
Błażejowski, M., Sikora, M., Moderski, R., & Madejski, G. M. 2000, ApJ, 545, 107
Błażejowski, M., et al. 2005, ApJ, 630, 130
Burrows, D. N., et al. 2005, Space Sci. Rev., 120, 165
Cardelli, J. A., Clayton, G. C., & Mathis, J. S. 1989, ApJ, 345, 245
Cash, W. 1979, ApJ, 228, 939
Celotti, A., Ghisellini, G., & Fabian, A. C. 2007, MNRAS, 375, 417
Chincarini, G., et al. 2003, Messenger, 113, 40
Covino, S., et al. 2004, Astron. Nachr., 325, 543
———. 2005, ATel, 564, 1
Dermer, C. D., & Atoyan, A. 2004, ApJ, 611, L9
Dermer, C. D., & Schlickeiser, R. 1993, ApJ, 416, 458
Dolcini, A., et al. 2005, A&A, 443, L33
Fuhrmann, L., et al. 2006, A&A, 445, L1
Fukugita, M., Shimasaku, K., & Ichikawa, T. 1995, PASP, 107, 945

Gehrels, N., et al. 2004, ApJ, 611, 1005
Ghisellini, G. 1989, MNRAS, 238, 449
———. 1999, Astron. Nachr., 320, 232
Ghisellini, G., Celotti, A., & Costamante, L. 2002, A&A, 386, 833
Ghisellini, G., Celotti, A., Fossati, G. Maraschi, L., & Comastri, A. 1998, MNRAS, 301, 451
Ghisellini, G., & Madau, P. 1996, MNRAS, 280, 67
Giommi, P., et al. 2006, A&A, 456, 911
Guetta, D., Ghisellini, G., Lazzati, D., & Celotti, A. 2004, A&A, 421, 877
Hartman, R. C., et al. 1999, ApJS, 123, 79
Hill, J. E., et al. 2004, Proc. SPIE, 5165, 217
Katarzyński, K., & Ghisellini, G. 2007, A&A, 463, 529
Kato, T., Kusunose, M., & Takahara, F. 2006, ApJ, 638, 653
Krawczynski, H., et al. 2004, ApJ, 601, 151
Massaro, E., Tramacere, A., Perri, M., Giommi, P., & Tosti, G. 2006, A&A, 448, 861
Moretti, A., et al. 2006, A&A, 448, L9
Murphy, E. M., Lockman, F. J., Laor, A., & Elvis, M. 1996, ApJS, 105, 369

Padovani, P., Giommi, P., Ábrahám, P., Csizmadia, S., & Moór, A. 2006, A&A, 456, 131
Pian, E., Falomo, R., & Treves, A. 2005, MNRAS, 361, 919
Pian, E., et al. 1998, ApJ, 492, L17
———. 1999, ApJ, 521, 112
———. 2002, A&A, 392, 407
———. 2006, A&A, 449, L21
Raiteri, C. M., et al. 2006, A&A, 459, 731
Roming, P. W. A., et al. 2005, Space Sci. Rev., 120, 95
Sambruna, R. M., et al. 2006, ApJ, 646, 23
Schlegel, D. J., Finkbeiner, D. P., & Davis, M. 1998, ApJ, 500, 525
Sikora, M., Begelman, M. C., & Rees, M. J. 1994, ApJ, 421, 153
Sokolov, A., & Marscher, A. P. 2005, ApJ, 629, 52
Spada, M., Ghisellini, G., Lazzati, D., & Celotti, A. 2001, MNRAS, 325, 1559
Tagliaferri, G., et al. 2003, A&A, 400, 477
Tramacere, A., et al. 2007, A&A, 467, 501
Treves, A., et al. 1993, ApJ, 406, 447
Ulrich, M.-H., Maraschi, L., & Urry, C. M. 1997, ARA&A, 35, 445
Zerbi, F. M., et al. 2001, Astron. Nachr., 322, 275